J Mol Model (2014) 20:2523
DOI 10.1007/s00894-014-2523-y

ORIGINAL PAPER

Quantum chemical investigation of the primary thermal pyrolysis reactions of the sodium carboxylate group in a brown coal model

Jian Li · Baisheng Zhang · Zhiqiang Zhang · Kefeng Yan · Lixun Kang

Received: 23 July 2014 / Accepted: 7 November 2014 / Published online: 2 December 2014

Abstract The primary pyrolysis mechanisms of the sodium carboxylate group in sodium benzoate—used as a model compound of brown coal—were studied by performing quantum chemical computations using B3LYP and the CBS method. Various possible reaction pathways involving reactions such as unimolecular and bimolecular decarboxylation and decarbonylation, crosslinking, and radical attack in the brown coal matrix were explored. Without the participation of reactive radicals, unimolecular decarboxylation to release CO_2 was calculated to be the most energetically favorable primary reaction pathway at the B3LYP/6-311+G (d, p) level of theory, and was also found to be more energetically favorable than decarboxylation of an carboxylic acid group. When CBS-QBS results were included, crosslinking between the sodium carboxylate group and the carboxylic acid and the decarboxylation of the sodium carboxylate group (catalyzed by the phenolic hydroxyl group) were found to be possible; this pathway competes with unimolecular decarboxylation of the sodium carboxylate group. Provided that H and CH_3 radicals are present in the brown coal matrix and can access the sodium carboxylate group, accelerated pyrolysis of the sodium carboxylate group becomes feasible, leading to the release of an Na atom or an $NaCO_2$ radical at the B3LYP/6-311+G (d, p) or CBS-QB3 level of theory, respectively.

Keywords Sodium carboxylate group · Pyrolysis · Quantum chemistry · Brown coal

Electronic supplementary material The online version of this article (doi:10.1007/s00894-014-2523-y) contains supplementary material, which is available to authorized users.

J. Li · B. Zhang · Z. Zhang (✉) · L. Kang
College of Mining Engineering, Taiyuan University of Technology, No.79 West Yingze Street, Taiyuan, Shanxi 030024, People's Republic of China
e-mail: donaldzhang@foxmail.com

K. Yan
Key Laboratory of Renewable Energy and Gas Hydrate, Guangzhou Institute of Energy Conversion, Chinese Academy of Sciences, Guangzhou 510640, People's Republic of China

K. Yan
Guangzhou Center for Gas Hydrate Research, Chinese Academy of Sciences, Guangzhou 510640, People's Republic of China

Introduction

When coal is heated to 200–300 °C, it undergoes pyrolysis. Thermochemical reactions that occur during pyrolysis include both bond-breaking and bond-forming reactions, which can decompose the macromolecular system of coal into smaller, useful hydrogen- and/or oxygen-rich products as well as aromatic units, until the coal comes to resemble a carbonaceous solid. This results in the formation of volatiles and nonvolatile char [1, 2]. An understanding of the pyrolysis behavior of coal is important because it is the initial thermochemical step in a number of processes applied to coal, including combustion, gasification, carbonization, and liquefaction.

Compared with higher-ranking coals, brown coal features a relatively low content of carbon and a high content of oxygen. The oxygen in brown coal exists in a wide variety of functional groups. Among them, carboxylic and phenolic functional groups constitute more than half of the oxygen-containing functional groups [3]. Due to their acidic nature, many of carboxylic acids in coal are present in carboxylate form, such as Na, Mg, and Ca carboxylates. These metallic species are clearly responsible for the characteristics of brown coal pyrolysis as well as subsequent gasification or combustion [4].

Among these metal components, the sodium originally associated with carboxylate undergoes volatilization during pyrolysis. This causes erosion and corrosion of turbine blades

during power generation from brown coal [5]. On the other hand, Na retained in the char following primary pyrolysis enhances gasification and combustion processes due to its catalytic activity. Its great importance has led to great efforts to understand how the presence of sodium carboxylate affects the pyrolysis of brown coal.

A large number of researchers have examined the roles of sodium carboxylate groups in the pyrolysis of brown coal. Experiments showed that the physicochemical form of sodium carboxylate changes with increasing temperature during pyrolysis. It is well known that decarboxylation of carboxylic groups plays an important role in the pyrolysis of brown coal [6]. Wornat et al. reported that, after sodium carboxylate has thermally decarboxylated and thus released CO_2 at <300 °C, the released sodium bonds to the remaining coal matrix [7]. Murry and Schafer et al. suggested that the sodium carboxylate group decomposes to Na_2CO_3 with the loss of CO_2 during pyrolysis at 400–600 °C [8, 9]. At higher temperatures, the bonds between the Na and coal/char matrix may break down thermally [4].

Studies also showed that the Na^+ in the sodium carboxylate group tends to suppress the yields of tar and total volatiles during pyrolysis, largely due to its transformation during pyrolysis [7, 10]. However, the exact roles played by the sodium carboxylate in the brown coal/char matrix during pyrolysis remain unclear, although there has been some speculation. Following studies on the gasification of the resulting char, Quyn et al. proposed [11] that the sodium carboxylate group in brown coal is likely to be bonded to O-containing structures in the char matrix after pyrolysis at low temperatures. As the pyrolysis temperature is increased, Na is increasingly likely to bond to C. Such bonds are considered to be much weaker than those between Na and O. However, contradictory results have also been reported in the literature. It was found that bonds between Na and the coal/char matrix become progressively stronger with increasing temperature during pyrolysis [10].

Additionally, the Na atom in sodium carboxylate is easily volatilized [12]. Indeed, there is discernible volatilization of Na during pyrolysis at temperatures as low as 300 °C [13]. However, the exact mechanism of the release of Na is unknown. It is believed [4] that one of the main steps in the volatilization of Na from sodium carboxylate at low temperatures is the direct volatilization of Na in the form of light carboxylates. As the temperature is increased further, some Na atoms may volatilize when CM–Na bonds (here, "CM" is the coal matrix) break and oxygen-containing species or aliphatic materials are released, although recombination of Na with free radicals in the coal matrix is also possible. Radicals also play essential roles in the volatilization of Na species. Interactions with H or other radicals in volatiles originating from brown coal pyrolysis are also considered to be responsible for the release of Na species, as they replace the Na species bonded to the char [14]. Direct release of Na is only observed to take place at temperatures >900 °C in the absence of radicals [10].

Although recent studies [15] have significantly contributed to our understanding of the role of Na-containing species during pyrolysis, the fundamental mechanisms associated with sodium carboxylate during the primary pyrolysis of brown coal are still poorly understood due to the complexity of the system. Further study is needed to fully assess the behavior of sodium carboxylate in brown coal during pyrolysis.

Quantum chemical methods have proven to be a powerful tool for improving our understanding of the process of pyrolysis at the molecular level. Computational molecular modeling has provided insights into the chemical transformations that occur during the pyrolysis of brown coal [16–18]. In previous work [19], we theoretically explored the thermal pyrolysis channels for the carboxylic group in selected molecular models. In the study reported in the present paper, we focused our research on the primary thermal pyrolysis of sodium carboxylate in brown coal. Possible reaction pathways involving the sodium carboxylate group were studied using model compounds by quantum chemical methods.

Modeling details

It is necessary to acknowledge the limitations faced by researchers developing a molecular model of brown coal: the size of the modeled molecule is restricted by the need to ensure that the associated density functional theory (DFT) computations are practicable. Very large molecular structures would require unrealistically large computational resources for high-level studies. Consequently, the size of the molecular model of brown coal must be restricted. Since brown coal is known to contain predominantly monoaromatic rings [20] and most of the carboxylic groups are associated with the aromatic rather than the aliphatic components [7], to simplify the calculations, the sodium carboxylate group in the brown coal was represented by a sodium benzoate model compound, as shown in Fig. 1.

It is well known that the abundant acidic functional groups in brown coal are carboxylic acid and phenolic hydroxyl groups. Hydrogen bonds may form between sodium carboxylate and these two groups, which may be an important influence on the pyrolysis behavior of the sodium carboxylate group [9]. Thus, aside from the self-pyrolysis reactions of isolated sodium carboxylate and sodium carboxylate dimers, the bimolecular pyrolysis behavior of sodium carboxylate associated with carboxylic acid and phenolic hydroxyl groups was also considered when choosing benzoic acid and phenol molecules as the molecular models of those groups in brown coal, respectively. In addition, free-radical reactions are ubiquitous in the thermal decomposition of coal, and often involve

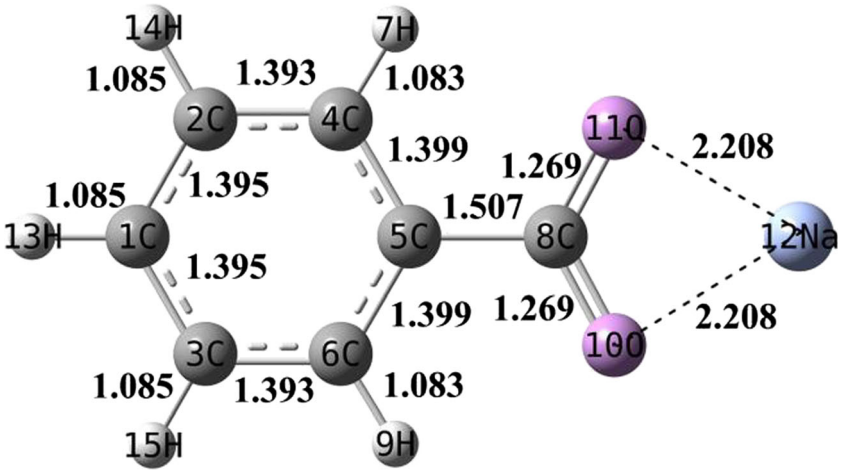

Fig. 1 Optimized geometry of sodium benzoate—employed as a model of brown coal with sodium carboxylate groups—calculated at the B3LYP/6-311 + G (d, p) level of theory (bond lengths in Å)

a number of elementary reactions in the overall mechanism. The evolutions of Na and light sodium carboxylates such as formate and acetate in the pyrolysis of brown coal have been observed experimentally, and may proceed via a radical mechanism [4]. Therefore, the possibility of radical reactions of sodium carboxylate groups in brown coal can also be explored using a sodium benzoate model.

Becke's three-parameter exchange functional and the Lee–Yang–Parr correlation functional (B3LYP) [21, 22] were used in all calculations here. All electronic and vibrational properties were calculated using the 6-311+G (d, p) basis set. This includes diffuse functions for heavy atoms and polarization for heavy and hydrogen atoms, both of which are necessary to perform calculations of charge-separated states. They are also required for radical structures with some atoms that have very large electron densities. The spin-unrestricted method was applied to the open-shell systems. Minimum-energy structures were achieved by allowing all of the geometric parameters to vary independently. We checked that the geometries corresponding to stable structures did not have imaginary vibration frequencies. The transition states (TS) were optimized using the synchronous transit-guided quasi-Newton (STQN) method [23, 24], and were identified by the presence of a single imaginary frequency. Further intrinsic reaction coordinate (IRC) calculations were performed, starting at the transition states, to verify that they connected the correct reactants and products [25]. Zero-point energy corrections (unscaled) were taken into account when evaluating the energies. High-accuracy complete basis set (CBS) methods [26] can remove the error that arises in quantum mechanical calculations from the truncation of basis sets. However, these methods are computationally expensive and completely unfeasible for calculations of even moderately large systems. Therefore, to evaluate the reliability of the B3LYP results, we only reoptimized the B3LYP/6-311+G (d, p) geometries of some relatively small systems using the CBS-QB3 method [27]; the energy values obtained using this method are shown in parentheses in the following text. The Gaussian 03 software package [28] was used for all of the quantum chemical calculations described above, with energy convergence (SCF=tight) specified.

Results and discussion

Unimolecular decarboxylation and decarbonylation

Both unimolecular decarboxylation and decarbonylation of sodium benzoate were proposed as processes, and the energetic profiles for these reaction pathways are shown in Scheme 1. The optimized lowest-energy conformation of the model reactant, sodium benzoate, is shown in Fig. 1. It is essentially a planar structure. The first reaction pathway is stepwise decarboxylation of sodium benzoate to form phenyl sodium and CO_2 (reaction 1). Figure 2 shows the energy diagram of this pathway. First, the CO_2 group in sodium benzoate twists by about 36° to form the reaction precursor IM1 via TS1-1 (Fig. 5), which has a torsional barrier of 19.3 (18.1) kcal mol^{-1}. After that, this precursor undergoes C5–C8 bond cleavage via TS1-2 (Fig. 5). The transition state TS1-2 corresponds to the development of negative charge on the evolving C_6H_5 moiety, which results in repulsion between the nascent CO_2 and the rest of the molecule. The bond with the sodium cation disperses some of the negative charge, and this cation stabilizes the transition state geometry by bonding to the departing components. The energy required to attain the transition state geometry from IM1 is 31.2 (45.8) kcal mol^{-1}. The second step in the decarboxylation of sodium benzoate is found to be the rate-determining step, regardless of whether the activation energy is caculated at the B3LYP/6-311+G (d, p) or the CBS-QB3 level of theory. The second possible reaction pathway for sodium benzoate is direct decarbonylation to form sodium phenolate and CO (reaction 2), with an activation energy of 91.0 (91.8) kcal mol^{-1} (Fig. 2)

Scheme 1 Proposed unimolecular decarboxylation and decarbonylation pathways of a sodium carboxylate group in brown coal

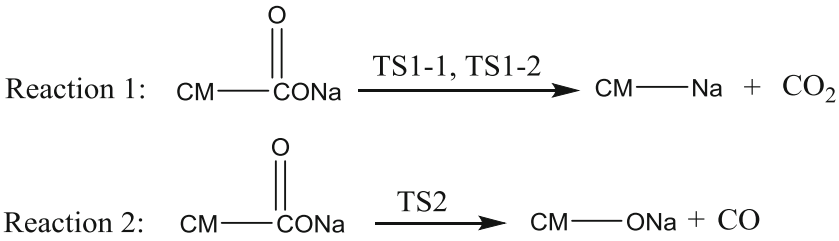

via TS2. Obviously, the activation energy of decarboxylation is considerably lower than that of decarbonylation, so the sodium carboxylate group should not decompose by decarbonylation to any significant extent in its isolated form at low temperature.

Domazetis et al. [16] have shown that the unimolecular decarboxylation is equally favored for both carboxylic acid and carboxylate, which is not consistent with our results. Our previous work indicated that for an isolated single carboxylic group in a brown coal model, unimolecular decarboxylation was possible via concerted or stepwise pathways, as both had similar activation energies (58.7 and 58.6 kcal mol^{-1}) when calculated at the B3LYP/6-311+G (d, p) level of theory [19]. These values are higher than that for the unimolecular decarboxylation of the sodium carboxylate group according to our present results. Therefore, the sodium carboxylate group should decarboxylate more readily than the carboxylic acid group in the brown coal matrix. This discrepancy may be due to the differences between the model and method used by Domazetis et al. and the model and method that we have used. The carboxylate model used by Domazetis et al. was a bare anion model with a charge of −1, which does not consider the influence of the metal cation. Moreover, the method used by them was a semiempirical quantum mechanical method, the accuracy of which is relatively low.

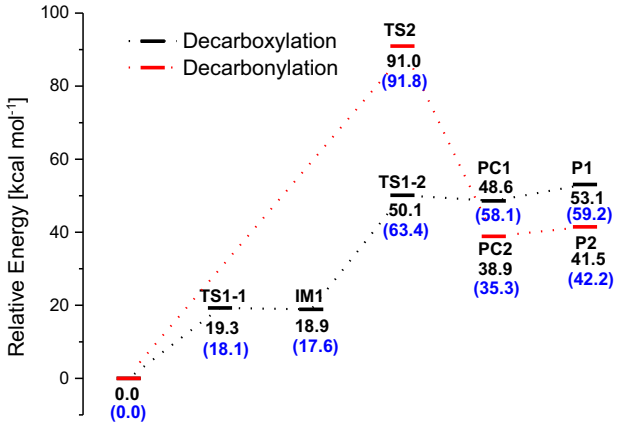

Fig. 2 Energy diagrams for decarboxylation (*black lines and dots*) and decarbonylation (*red lines and dots*) of the sodium benzoate model. Energy values (in kcal mol^{-1}) without parentheses were obtained at the B3LYP/6-311 + G (d, p) level of theory, whereas those in parentheses were calculated at the CBS-QB3 level of theory

Bimolecular decarboxylation, decarbonylation, and crosslinking

The next step in this computational study was to investigate the bimolecular catalytic decompositions (decarboxylation and decarbonylation) and crosslinking of the sodium carboxylate group in brown coal using sodium benzoate and related model compounds (benzoic acid and phenol). Considering that CBS calculations of large molecule systems are prohibitively expensive, only the B3LYP method was used to explore these reactions. Based on the reaction scheme outlined above (Scheme 2), nine possible reaction pathways were considered. Reactions 3, 4, and 5 show the decarboxylation, decarbonylation, and crosslinking of the sodium benzoate dimer, respectively. Figures 3a and 5 show the relative energies and the transition state structures (TS3, TS4, and TS5) of these reactions. The pre-reaction complexes (RC3, RC4, and RC5, respectively) are initially formed in these three reactions; in each case, the stabilization energy is about 40 kcal mol^{-1}. In the catalytic decarboxylation pathway, electrophilic attack by the sodium cation of the first sodium benzoate on the C5 atom of the second sodium benzoate results in the displacement of the CO_2 of the second sodium benzoate through the cleavage of the C5–C8 bond that anchors the CO_2 group. After the detachment of CO_2 from the second sodium benzoate model, Na–Na exchange occurs, leading to the formation of phenyl sodium. The activation barrier to this reaction is 56.7 kcal mol^{-1}. Catalytic decarbonylation of the sodium carboxylate group via Na–Na exchange (reaction 4 in Scheme 2) was also considered. The energy barrier to this reaction was calculated to be 92.8 kcal mol^{-1}. It has also been proposed that decarboxylation reactions are major contributors to the crosslinking processes observed during the thermal processing of brown coal [29, 30]. However, in our previous study [19] we found that dehydration and esterification of the carboxylic aicd group contributed to low-temperature crosslinking. In this work, the possible crosslinking reaction of the sodium carboxylate group dimer was investigated (reaction 5). This reaction leads to the formation of anhydride and Na_2O adduct, and involves the transition state TS5 (Fig. 5) with an activation barrier of 134.2 kcal mol^{-1}. Upon comparing the energy barriers of the above three reactions, it is easy to see from Fig. 3a that the energy barrier of reaction 3 (56.7 kcal mol^{-1}) is the lowest.

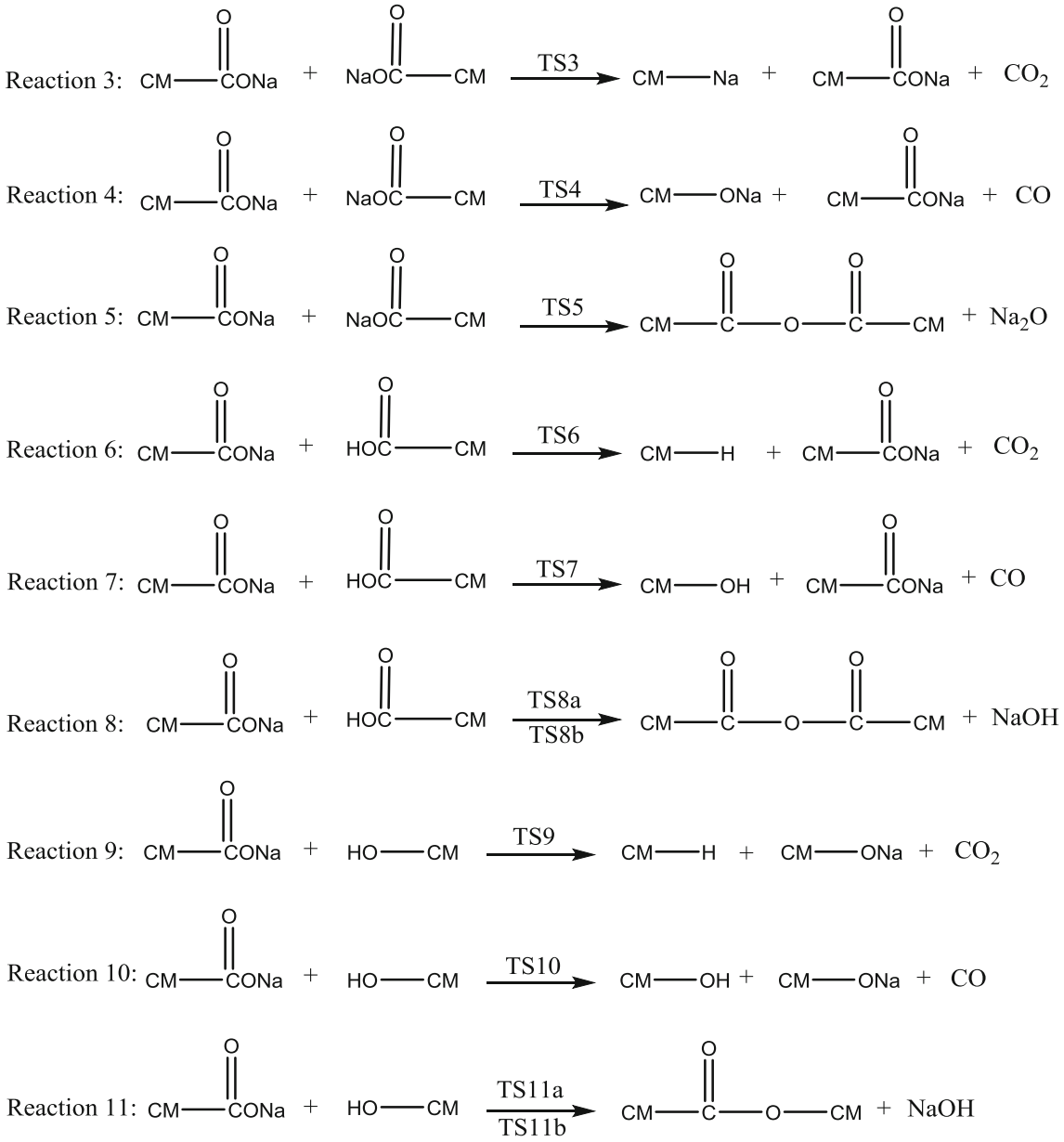

Scheme 2 Proposed bimolecular decarboxylation, decarbonylation, and crosslinking pathways of a sodium carboxylate group in brown coal

Bimolecular decarboxylation, decarbonylation, and crosslinking (reactions 6, 7, and 8 in Scheme 2) may also occur between neighboring sodium carboxylate and carboxylic acid groups. Figure 3b shows the potential energy profiles along these three possible reaction pathways. It can be seen from Scheme 2 and Fig. 3b that, catalyzed by the neighboring sodium carboxylate group (reaction 6) via Na–H exchange, the model compound sodium benzoate decarboxylates and thus releases CO_2. The energy barrier to this decarboxylation is 50.9 kcal mol^{-1}. The possible catalytic decarbonylation of the sodium carboxylate group via Na–H exchange in the brown coal matrix (reaction 7) was also considered. This process was calculated to be exothermic by 25.5 kcal mol^{-1}, and to lead to the formation of the pre-reaction complex RC7, which is the same as that (RC6) involved in reaction 6. RC7 then decarbonylates to release CO via TS7 (barrier height: 94.9 kcal mol^{-1}). Crosslinking between sodium carboxylate and carboxylic acid groups in brown coal (reaction 8) is also conceivable. Using sodium benzoate and benzoic acid as the model compounds for these two groups, two possible crosslinking routes were investigated. The first occurs via the cleavage of the C8–O10 or C8–O11 bond of sodium benzoate and the O–H bond of benzoic acid via TS8a. The second can occur via the cleavage of the O10–Na12 or O11–Na12 bond of sodium benzoate and the C–O bond of benzoic acid via TS8b. These two processes were calculated to be exothermic by 14.2 and 8.8 kcal mol^{-1}, and to result in the formation of the pre-reaction complex RC8a or RC8b,

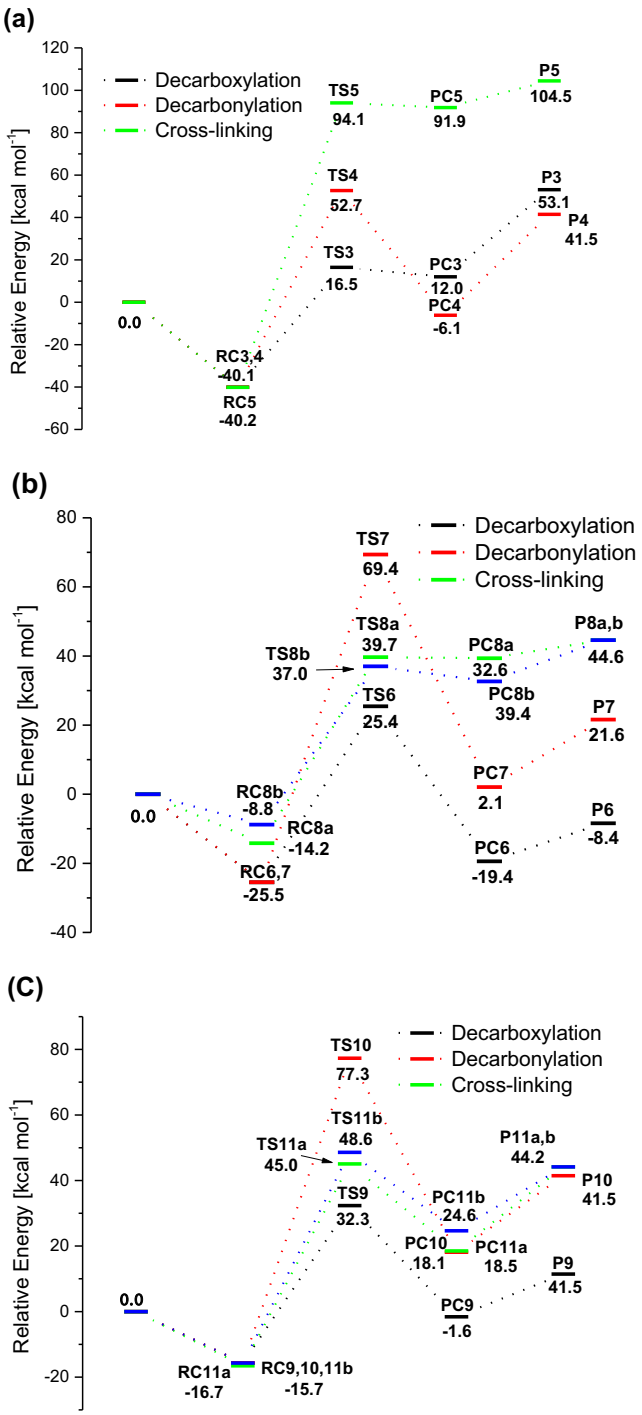

Fig. 3a–c Energy diagrams for the bimolecular decarboxylation (*black lines and dots*), decarbonylation (*red lines and dots*), and crosslinking (*green lines and dots*) pathways of sodium benzoate dimer (**a**), sodium benzoate + benzoic acid (**b**), and sodium benzoate + phenol (**c**), calculated at the B3LYP/6-311 + G (d, p) level of theory (energy scale in kcal mol^{-1})

respectively. The barriers to the transition states TS8a and TS8b are 53.9 and 45.8 kcal mol^{-1}, respectively. Upon comparing the stabilities of the pre-reaction complexes and the energy barrier heights of all four possible reactions between sodium carboxylate and carboxylic acid groups (Fig. 3b), it is clear that the crosslinking pathway is favored.

Figure 3c illustrates the potential surfaces for bimolecular decarboxylation, decarbonylation, and crosslinking (reactions 9, 10, and 11 in Scheme 2) between a sodium carboxylate group and a neighboring phenolic acid group in the brown coal matrix. The calculated geometries and energies of their pre-reaction complexes (RC9, 10, 11a, and 11b) are similar. The catalytic decarboxylation and decarbonylation of sodium carboxylate via Na–H exchange (reactions 9 and 10) proceed via the transition states TS9 and TS10 (as shown in Fig. 5). The calculated activation barriers to these two reactions are 48.0 and 93.0 kcal mol^{-1}, respectively. Esterification crosslinking between sodium carboxylate and phenolic hydroxyl groups was also considered (reaction 11). Two possible reaction routes were proposed. In the first, crosslinking is achieved via the elimination of the O10–Na12 or O11–Na12 group of sodium benzoate and a proton from phenol; the activation barrier to this is 61.6 kcal mol^{-1} (Fig. 3c). The second reaction mechanism assumes direct formation of NaOH (barrier: 64.3 kcal mol^{-1}) through the combination of the Na cation of the sodium carboxylate group of sodium benzoate with the hydroxyl group of phenol as well as C–O bond formation (i.e., in the ester group). Comparison of the three types of bimolecular reactions discussed above suggests that the lowest-energy pathway is the catalytic decarboxylation of sodium benzoate via reaction 9.

The activation barriers and reaction enthalpies at 0 K of the predominant unimolecular and bimolecular pathways of the sodium carboxylate group in the brown coal model are summarized in Table 1. From Table 1, it is apparent that the energy barrier to unimolecular decarboxylation (reaction 1) is the lowest when calculated at the B3LYP/6-311+G (d, p) level of theory. This means that none of the intermolecular complexes, including those with an adjacent sodium carboxylate, carboxylic acid, or phenolic hydroxyl group, enhance the thermal decomposition of sodium carboxylate groups in the brown coal matrix. However, the CBS-QB3 method predicts a higher barrier height (45.8 kcal mol^{-1}) in the rate-determining step of unimolecular decarboxylation (reaction 1), which is equal to that of reaction 8 and also very close to that of reaction 9 when computed at the B3LYP/6-311+G (d, p) level. Unfortunately, because the computationally expensive CBS composite method cannot be used in these bimolecular reactions, direct comparison with CBS-QB3 results is impossible in the present work. That said, the results calculated here still indicate that the formation of dimeric sodium carboxylate groups cannot accelerate carboxylate decomposition (bimolecular decarboxylation, decarbonylation, or crosslinking), in contrast to carboxylic acid group decomposition in brown coal [19]. Therefore, the complexed binary adduct of sodium carboxylate groups would appear to undergo unimolecular decarboxylation, leading to the release of CO_2, in the primary

Table 1 Activation barriers and reaction enthalpies at 0 K of the predominant reaction pathways of a sodium carboxylate group in brown coal model

Reaction	Mechanism	Activation barrier (kcal mol^{-1})		Reaction energy (kcal mol^{-1})	
		B3LYP/6-311+G (d, p)	CBS-QB3	B3LYP/6-311+G (d, p)	CBS-QB3
Sodium benzoate: reaction 1	Unimolecular decarboxylation	31.2	45.8	53.1	58.1
Sodium benzoate dimer: reaction 3	Catalytic decarboxylation	56.7		53.1	
Sodium benzoate + benzoic acid: reaction 8	Crosslinking	45.8		44.6	
Sodium benzoate + phenol: reaction 9	Catalytic decarboxylation	48.0		11.5	

pyrolysis process prior to bimolecular reactions in the brown coal matrix. However, when the sodium carboxylate group can form a binary complex with a carboxylic acid group, unimolecular decarboxylation of the sodium carboxylate group and crosslinking between sodium carboxylate and carboxylic acid groups to form NaOH may be equally favored. In addition, catalytic decarboxylation may occur to some extent provided a hydrogen-bonded pre-reaction complex can form between sodium carboxylate and phenolic hydroxyl groups in the brown coal matrix.

Radical reaction mechanism

We first inspected the possibility of direct cleavage of the O–Na and C5–C8 bonds in the sodium carboxylate group to form an Na atom and an $NaCO_2$ radical using the sodium benzoate model. Transition states were not found in these bond dissociation processes when potential energy surface (PES) scans of O–Na and C5–C8 bonds were performed at the B3LYP/6-311+G (d, p) level. Thus, bond dissociation energies (BDEs) were computed using the methodology reported by Blanksby and Ellison [31], which was developed for systems which undergo unimolecular reactions that lack a well-defined transition state. Unfortunately, as the experimental BDE values of these reactions are unavailable in the literature, direct comparison between experiment and theory is not possible. In order to check the reliability of the B3LYP/6-311+G (d, p) method, the highly accurate CBS-QB3 method was also used. These calculated BDE values are collected in Table 2. From Table 2, it can be seen that the BDEs (94.6 kcal mol^{-1} for O–Na rupture and 91.9 kcal mol^{-1} for C5–C8 rupture) computed at the B3LYP/6-311+G (d, p) level are lower than those (102.4 kcal mol^{-1} for O–Na rupture and 103.9 kcal mol^{-1} for C5–C8 rupture) computed at the CBS-QB3 level. Nevertheless, these values are far higher than the barriers to the rate-determining steps in the predominant unimolecular and bimolecular reactions mentioned above, indicating that these dissociation reactions are of minor importance in the primary thermal pyrolysis of sodium carboxylate groups in brown coal at low temperatures [10].

The BDEs of C–H bonds in the sodium benzoate model were also calculated at the B3LYP/6-311+G (d, p) and CBS-QB3 levels of theory and are shown in Table 2. The BDE values computed at the CBS-QB3 level are very close to the experimental value (111.3 kcal mol^{-1}) for a similar compound, benzene [32], demonstrating that the CBS model can accurately reproduce experimental thermodynamic data. Although the BDEs of C–H bonds at the *ortho*, *meta*, and *para* positions computed at the B3LYP/6-311+G (d, p) level were 4.7, 4.9, and 4.9 kcal mol^{-1}, respectively, lower than those computed at the CBS-QB3 level, they are still far higher than the activation energies for the dominant pyrolysis pathways of sodium carboxylate groups in the brown coal matrix. Thus, compared with the pyrolysis of the sodium carboxylate group in the sodium benzoate model, the rupture of C–H bonds is less likely to occur during the primary pyrolysis of sodium carboxylate groups in the brown coal matrix.

Although the pyrolysis of the sodium carboxylate group to form radicals at low temperatures is not supported by the results of our study, reactive radicals have been reported in brown coal at such temperatures—even at room temperature [33]. Additionally, prior to the decomposition of the sodium carboxylate group, inherently weak bonds in the coal matrix may undergo thermolysis upon heating, generating radicals. It would be intriguing to know if these radicals can initiate the

Table 2 BDEs for the thermal decomposition of the model compound sodium benzoate, calculated at the B3LYP/6-311+G (d, p) and CBS-QB3 levels of theory

Reaction	BDE (kcal mol^{-1})	
	B3LYP/6-311+G (d, p)	CBS-QB3
$C_6H_5COONa = C_6H_5COO + Na$	94.6	102.4
$C_6H_5COONa = C_6H_5 + COONa$	91.9	103.9
$C_6H_5COONa = o\text{-}C_6H_4COONa + H$	110.0	114.7
$C_6H_5COONa = m\text{-}C_6H_4COONa + H$	108.5	113.4
$C_6H_5COONa = p\text{-}C_6H_4COONa + H$	108.7	113.6

reaction of the sodium carboxylate group during pyrolysis. However, since the free-radical sites attached to the bulky aromatic ring framework in the solid coal matrix are well separated in brown coal due to steric hindrance, it is not easy for them to combine with sodium carboxylate groups. Only small radicals such as H and CH_3 can readily penetrate into the coal matrix [34] and combine with sodium carboxylate groups during pyrolysis. Therefore, rather than detailing every reaction for all possible radicals, in this work we focused on reactions between H and CH_3 radicals and a sodium carboxylate group in this study.

Three reaction channels between an H radical and a sodium carboxylate group (reactions 12, 13, and 14 in Scheme 3) were proposed in this study. Figure 4a shows the energy profiles calculated at the B3LYP/6-311+G (d, p) level. These processes start with an H radical approaching different active sites on sodium benzoate, leading to the formation of various pre-reaction complexes (RC12, 13, and 14), the geometries of which are shown in Fig. 6. The structures of RC12 and RC13 are similar due to the adsorption of the H radical at the O10 or (the equivalent) O11 atom, respectively, while the H radical is adsorbed on the surface of the aromatic ring in RC14. From Fig. 4a, it can been seen that the formation of each of the three reactant complexes is exothermic, and the adsorption energies of reactions 12, 13, and 14 were computed as 0.3, 0.3, and 0.2 kcal mol^{-1} at the B3LYP/6-311+G (d, p) level, respectively, meaning that the systems can be stabilized by collisions. These three values are very close to each other, indicating there is no strongly preferred adsorption site of the H radical.

Subsequently, the displacement of Na from sodium carboxylate in the coal matrix by an H radical (reaction 12) was investigated. Figure 7 shows the transition state geometry (TS12) of this reaction. It can be seen that the replacement of Na by an H radical has a small energy barrier of 2.3 kcal mol^{-1} when calculated at the B3LYP/6-311+G (d, p) level. In addition, an H radical can also attack C8 of the carboxylate to form a sodium formate molecule (reaction 13) or attack the aromatic C5 to form an $NaCO_2$ radical (reaction 14). Calculations indicate that both of these reactions proceed via stepwise addition–elimination mechanisms. The transition-state geometries (TS13-1 and TS13-2) of the former reaction are also shown in Fig. 7. The first step in this reaction is the adsorption of the radical at the C8 atom with an activation energy of 11.6 kcal mol^{-1}. The second step is the release of sodium formate and a phenyl radical with an activation energy of 4.8 kcal mol^{-1}. Comparing the heights of the activation barriers encountered during this route, it is easy to discern that the first step is the rate-determining step. The latter reaction also proceeds via two transition state geometries (TS14-1 and TS14-2 as shown in Fig. 7) in a similar manner, but the first step is the addition of an H radical to the aromatic C5 atom and the second step leads to the formation of an $NaCO_2$ radical. It is worth noting that the released $NaCO_2$

Scheme 3 Proposed reaction pathways of H and CH_3 radicals with a sodium carboxylate group in brown coal

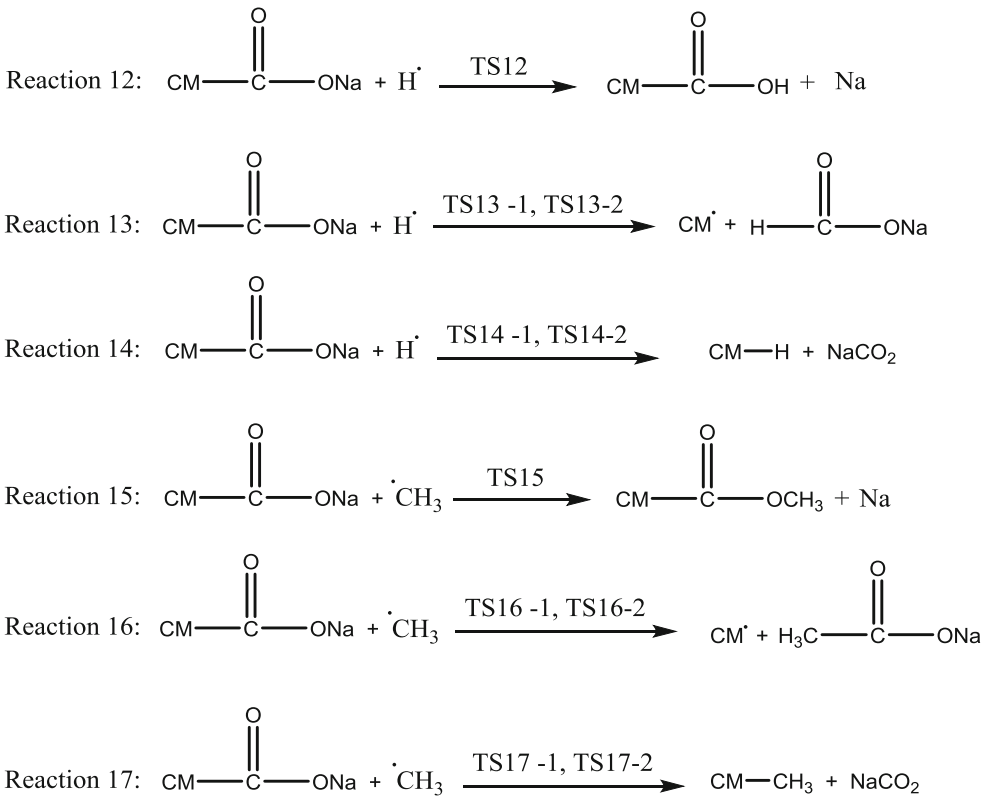

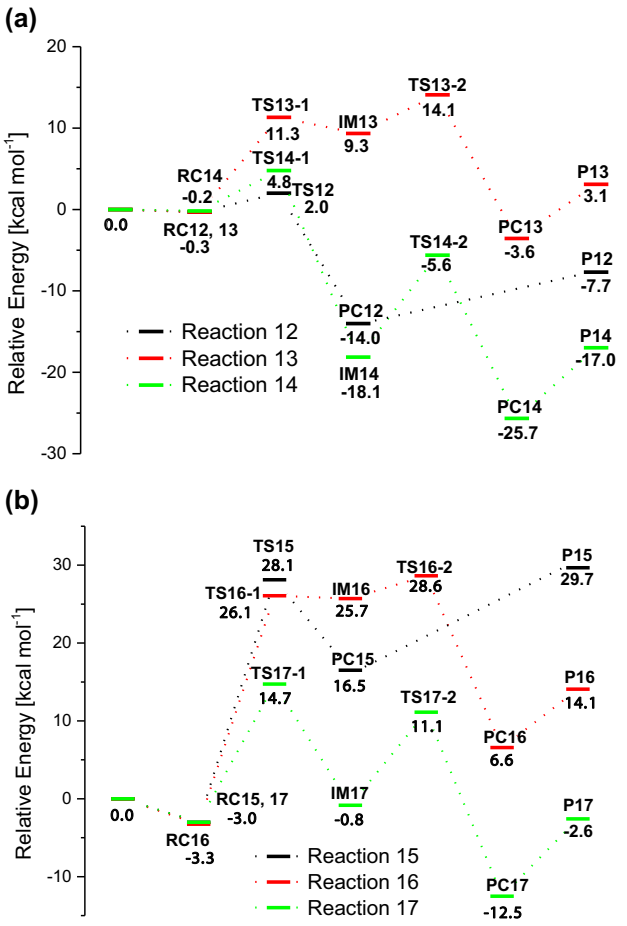

Fig. 4a–b Energy diagrams for the reactions of H (**a**) and CH_3 (**b**) radicals with the sodium benzoate model, calculated at the B3LYP/6-311 + G (d, p) level of theory (energy scale in kcal mol^{-1})

radical may split into an Na atom and a CO_2 molecule during the secondary reaction. The second step is the rate-determining step due to its higher activation barrier height (12.5 kcal mol^{-1}) than that of the first step (5.0 kcal mol^{-1}). The values of the activation barriers obtained for H-radical addition-displacement via different pathways clearly indicate that the replacement of Na by an H radical (reaction 12) is the most energetically favored route.

The possible pathways for the reaction between a CH_3 radical and a sodium carboxylate group (reactions 15, 16, and 17 in Scheme 3) share some similarities with those of an H radical and a sodium carboxylate group, as shown in Fig. 4b. It can be seen that the energies of pre-reaction complexes RC15, 16, and 17 are nearly the same when calculated at the B3LYP/6-311+G (d, p) level. The adsorption energies of both RC15 and 17 are 3.0 kcal mol^{-1} while the energy of RC16 is 3.3 kcal mol^{-1} lower than the reactants (a CH_3 radical and the sodium benzoate model compound), indicating that all three pre-reaction complexes are almost equally favored. The slight energy difference comes from the different geometries of the pre-reaction complexes. Figure 6 illustrates the geometries of RC15, 16, and 17. From Fig. 6, it can be seen that the geometries of RC15 and 17 are basically the same, whereas the geometry of RC16 is different, especially the orientation of the CH_3 radical. Reaction 17 has a 17.7 kcal mol^{-1} barrier at TS17-1 (Fig. 4b) associated with the rate-determining step, which is much lower than those of reactions 15 (31.1 kcal mol^{-1}) and 16 (29.3 kcal mol^{-1} for the rate-determining step), showing that reaction 17 is more favorable. However, this attack of the CH_3 radical at C5 in the sodium benzoate model (reaction 17) leads to the release of $NaCO_2$, which is different to the release of an Na atom in the preferred H-radical displacement reaction (reaction 12) described above. In addition, the binding energy of RC17 relative to the reactants (CH_3 and sodium benzoate) is higher than that of RC12 in reaction 12 (the predominant pathway for H-radical attack); that is, RC17 is less stable than RC12. It should be noted that these H and CH_3 radical reaction pathways are both temperature and pressure dependent from a kinetics perspective, as they proceed through a chemically activated intermediate, which would substantially influence all of these radical reaction processes.

In addition, to support the above findings, CBS-QB3 calculations were also performed to evaluate the activation barrier. Table 3 summarizes results for the barrier height relative to the pre-reaction complex calculated at the B3LYP/6-311+G (d, p) and CBS-QB3 levels. From Table 3, it can be seen that the results obtained with the B3LYP/6-311+G (d, p) method have a mean absolute deviation of 3.0 kcal mol^{-1} when compared to those afforded by CBS-QB3. Nevertheless, the dominant pathways for H and CH_3 radical reactions are still reactions 12 and 17 at the CBS-QB3 level of theory, in agreement with the B3LYP/6-311+G (d, p) results. However, the calculated activation barriers for reaction 17 indicate that, at the CBS-QB3 level, the second step is the rate-determining step, whereas the first step is the rate-determining step at the B3LYP/6-311+G (d, p) level, as shown in Table 3 (Fig. 7).

To gain more confidence in the performance of the B3LYP/6-311+G (d, p) method applied to these H and CH_3 radical reaction pathways, a comparison between the barrier yielded by B3LYP/6-311+G (d, p) and the corresponding experimentally measured value of this barrier is needed. However, there is no report in the literature of experimental measurements of reactions of H and CH_3 radicals with sodium benzoate, so we must use experimental results for a similar compound instead. Such results for the reaction of an H radical with phenol:

$$H\cdot + C_6H_5OH = C_6H_6 + \cdot OH,$$

which is similar to reaction 14, were found in the literature [35]. The measured activation barrier (7.9 kcal mol^{-1}) of the former reaction is in moderately good agreement with the calculated barrier height of the rate-determining step in reaction 14, supporting the applicability of the B3LYP/6-311+G (d, p) method to these reactions.

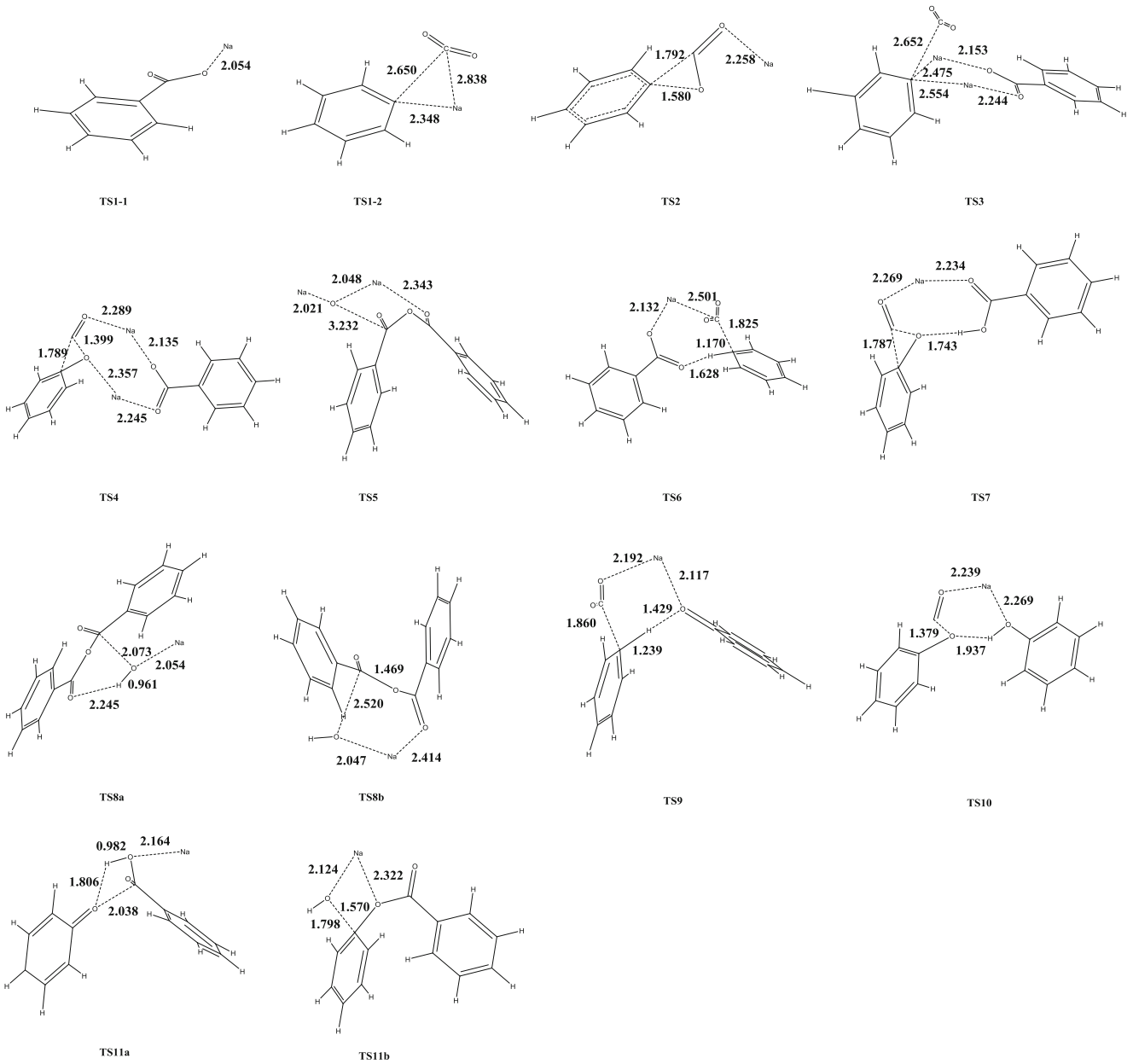

Fig. 5 Optimized geometries of transition states in the unimolecular decarboxylation (TS1-1 and TS1-2) and decarbonylation (TS2) of sodium benzoate, the bimolecular decarboxylation (TS3), decarbonylation (TS4), and crosslinking (TS5) of a sodium benzoate dimer, the bimolecular decarboxylation (TS6), decarbonylation (TS7), and crosslinking (TS8a and TS8b) of sodium benzoate + benzoic acid, and the bimolecular decarboxylation (TS9), decarbonylation (TS10), and crosslinking (TS11a and TS11b) of sodium benzoate + phenol, calculated at the B3LYP/6-311 + G (d, p) level of theory

Finally, the probability of an H or a CH_3 radical combining with the Na in the carboxylate group to form NaH or $NaCH_3$ was also investigated. Calculations performed at the B3LYP/6-311+G (d, p) level showed no discernable energy maximum via the synchronous transit-guided quasi-Newton method or a PES scan across the bond Na12–C8 or the distance between Na and the H (CH_3) radical in the pre-reaction complex. Thus, the dissociation of NaH or $NaCH_3$ from pre-reaction complexes of an H or a CH_3 radical with sodium benzoate may be barrierless reactions but they are very endothermic with respect to other H and CH_3 radical reactions. It was found that 51.2 and 65.1 kcal mol^{-1} are needed to accomplish these two reactions when they were calculated at the B3LYP/6-311+G (d, p) level, while CBS-QB3 gave more endothermic reaction energies (59.1 and 71.9 kcal mol^{-1}) than the B3LYP method. Thus, this route requires much more energy than the favorable radical reaction discussed above, and may be ruled out at low temperatures.

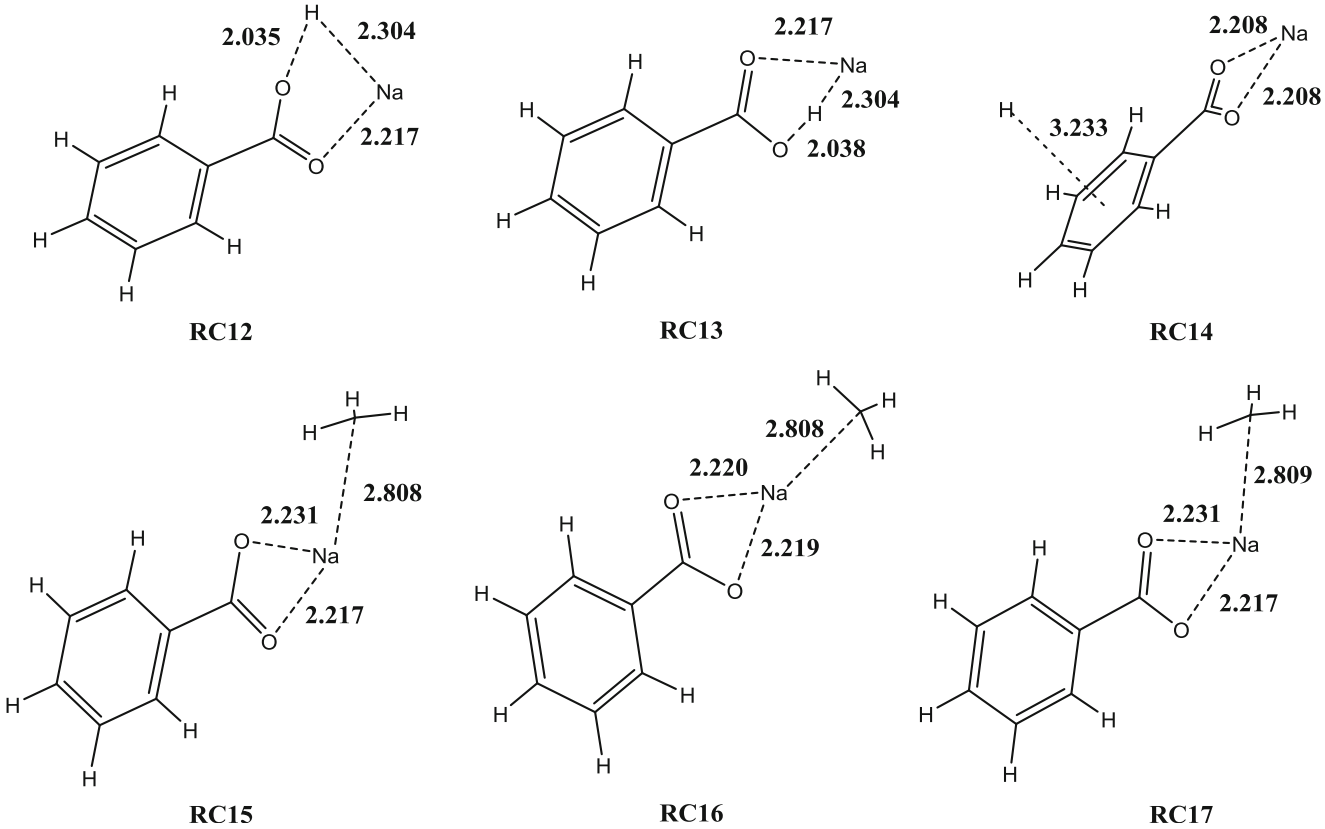

Fig. 6 Optimized geometric structures of pre-reaction complexes associated with H and CH_3 radical attack on the sodium benzoate model

Compared with unimolecular decarboxylation (reaction 1), bimolecular crosslinking (reaction 8), and catalytic decarboxylation (reaction 9) of the sodium benzoate model in brown coal, which are the preferred primary pyrolysis pathways that do not involve free radicals, the reactions involving H and CH_3 radicals proceed with much lower activation barriers. However, the predominant radical pathways of these two reactions are different. The presence of an H radical can enhance the release of an Na atom from brown coal, while the presence of a CH_3 radical can increase the likelihood of $NaCO_2$ radical formation [36]. The favorability of these processes should be determined by the relative abundances and availabilities of H and CH_3 radicals within the brown coal matrix. Among the unimolecular, bimolecular, and radical decomposition mechanisms that are possible for the sodium carboxylate group, the radical mechanisms should be favored provided that H and CH_3 radicals are abundant in the coal and can access sodium carboxylate groups.

Table 3 Calculated activation barriers for reactions involving the attack of an H or a CH_3 radical on the model compound sodium benzoate (Scheme 3), as calculated at the B3LYP/6-311+G (d, p) and CBS-QB3 levels of theory

Reaction		Activation barrier (kcal mol^{-1})	
		B3LYP/6-311+G (d, p)	CBS-QB3
Reaction 12		2.3	4.0
Reaction 13	First step	11.6	12.9
	Second step	4.7	5.8
Reaction 14	First step	5.0	7.5
	Second step	12.5	16.7
Reaction 15		31.1	28.7
Reaction 16	First step	29.3	23.9
	Second step	2.9	5.6
Reaction 17	First step	17.7	13.7
	Second step	12.0	16.6

Conclusions

The reaction mechanisms involved in the primary pyrolysis of sodium carboxylate groups in brown coal were studied using density functional theory and the CBS-QB3 method. These theoretical calculations provided mechanistic details about the unimolecular direct decarboxylation and decarbonylation of sodium carboxylate groups. Additionally, possible bimolecular reactions with neighboring functional groups were investigated to evaluate their feasibility, including decarboxylation, decarbonylation, and crosslinking reactions of complex systems such as a dimeric sodium carboxylate group, the

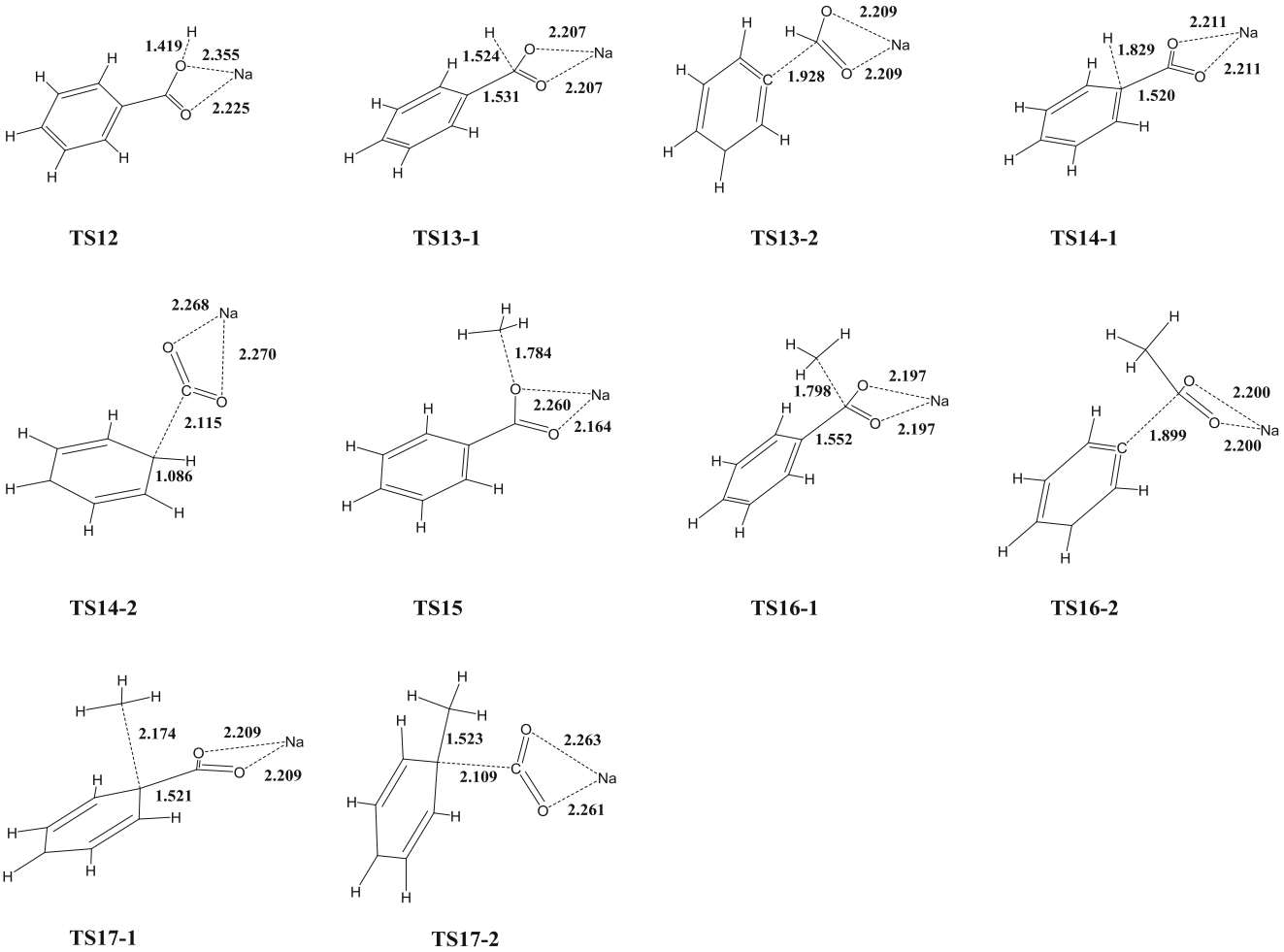

Fig. 7 Optimized geometries of transition states for the reactions of H (TS12, TS13-1, TS13-2, TS14a, and TS14b) and CH_3 (TS15, TS16-1, TS16-2, TS17-1, and TS17-2) radicals with sodium benzoate, calculated at the B3LYP/6-311+G (d, p) level of theory

hydrogen-bonded complex of a sodium carboxylate group with a carboxylic acid group, and phenolic hydroxyl groups in the brown coal matrix. The results of calculations performed at the B3LYP/6-311+G (d, p) level indicated that unimolecular decarboxylation of the sodium carboxylate group to release CO_2 is the favored primary pyrolysis route provided that radicals are not involved. Decomposition or crosslinking of the dimeric sodium carboxylate group is discouraged due to high energy barriers. Additionally, unimolecular decarboxylation of a sodium carboxylate group was found to be more energetically favorable than that of a carboxylic acid group. However, when the height of the barrier to unimolecular decarboxylation was evaluated at the CBS-QB3 level of theory, it was apparent that crosslinking between sodium carboxylate and carboxylic acid groups and decarboxylation of the sodium carboxylate group catalyzed by a neighboring phenolic hydroxyl group can also occur to some extent provided that a hydrogen-bonded pre-reaction complex can form between them in the brown coal matrix. Results calculated at both the B3LYP/6-311+G (d, p) and CBS-QB3 levels also showed that, assuming that H and CH_3 radicals are available and accessible, these radicals can decrease the activation energy for the pyrolysis of a sodium carboxylate group in the brown coal matrix, leading to the release of an Na atom and an $NaCO_2$ radical, respectively.

Acknowledgments Financial support from the National Natural Science Foundation of China (no. 51404162) is gratefully acknowledged.

References

1. Morgan TJ, Kandiyoti R (2014) Chem Rev 114:1547–1607
2. Solomon PR, Serio MA, Suuberg EM (1992) Prog Energy Combust Sci 18:133–220
3. Schafer HNS (1970) Fuel 49:197–213
4. Quyn DM, Wu H, Bhattacharya SP, Li C-Z (2002) Fuel 81:151–158
5. Takematsu T, Maude C (1991) Coal gasification for IGCC power generation. Gemini House, London
6. Eskay TP, Britt PF, Buchanan AC (1996) Energy Fuel 10:1257–1261
7. Wornat MJ, Sakurovs R (1996) Fuel 75:867–871

8. Murray JB (1973) Fuel 52:105–111
9. Schafer HNS (1979) Fuel 58:667–672
10. Li CZ, Sathe C, Kershaw JR, Pang Y (2000) Fuel 79:427–438
11. Quyn DM, Wu H, Hayashi J-i, Li C-Z (2003) Fuel 82:587–593
12. van Eyk PJ, Ashman PJ, Nathan GJ (2011) Combust Flame 158: 2512–2523
13. Sathe C, Pang Y, Li C-Z (1999) Energy Fuel 13:748–755
14. Wu H, Quyn DM, Li C-Z (2002) Fuel 81:1033–1039
15. Li CZ (2007) Fuel 86:1664–1683
16. Domazetis G, Raoarun M, James BD (2006) Energy Fuel 20:1997–2007
17. Yan G, Zhang Z, Yan K (2013) Mol Phys 111:147–156
18. Mathews JP, van Duin ACT, Chaffee AL (2011) Fuel Process Technol 92:718–728
19. Liu S, Zhang Z, Wang H (2012) J Mol Model 18:359–365
20. Hatcher PG, Breger IA, Szeverenyi N, Maciel GE (1982) Org Geochem 4:9–18
21. Kim K, Jordan KD (1994) J Phys Chem 98:10089–10094
22. Stephens PJ, Devlin FJ, Chabalowski CF, Frisch MJ (1994) J Phys Chem 98:11623–11627
23. Peng C, Ayala PY, Schlegel HB, Frisch MJ (1996) J Comput Chem 17:49–56
24. Peng C, Schlegel HB (1993) Israel J Chem 33:449–454
25. Gonzalez C, Schlegel HB (1990) J Phys Chem 94:5523–5527
26. Petersson GA, Bennett A, Tensfeldt TG, Al-Laham MA, Shirley WA, Mantzaris J (1988) J Chem Phys 89:2193–2218
27. Montgomery JA, Frisch MJ, Ochterski JW, Petersson GA (1999) J Chem Phys 110:2822–2827
28. Klene M, Li X, Knox JE, Hratchian HP, Cross JB, Adamo C, Jaramillo J, Gomperts R, Stratmann RE, Yazyev O, Austin AJ, Cammi R, Pomelli C, Ochterski JW, Ayala PY, Morokuma K, Voth GA, Salvador P, Dannenberg JJ, Zakrzewski VG, Dapprich S, Daniels AD, Strain MC, Farkas O, Malick DK, Rabuck AD, Raghavachari K, Foresman JB, Ortiz JV, Cui Q, Baboul AG, Clifford S, Cioslowski J, Stefanov BB, Liu G, Liashenko A, Piskorz P, Komaromi I, Martin RL, Fox DJ, Keith T, Al-Laham MA, Peng CY, Nanayakkara A, Challacombe M, Gill PMW, Johnson B, Chen W, Wong MW, Gonzalez C, Pople JA (2003) Gaussian 03, revision A.1. Gaussian Inc., Pittsburgh
29. Ibarra J, Moliner R, Gavilan MP (1991) Fuel 70:408–413
30. Joseph JT, Forrai TR (1992) Fuel 71:75–80
31. Blanksby SJ, Ellison GB (2003) Acc Chem Res 36:255–263
32. Ervin KM, DeTuri VF (2002) J Phys Chem A 106:9947–9956
33. Czechowski F, Jezierski A (1997) Energy Fuel 11:951–964
34. Smith GV, Wiltowski T, Phillips JB (1989) Energy Fuel 3: 536–537
35. He YZ, Mallard WG, Tsang W (1988) J Phys Chem 92:2196–2201
36. Zhang S, Hayashi J-i, Li C-Z (2011) Fuel 90:1655–1661